25th AIAA Aerodynamic Measurement Technology and Ground Testing Conference
5 - 8 June 2006, San Francisco, California

AIAA 2006-3291

AIAA 2006–3291

Applications of CFD Analysis in Arc-Jet Testing of RCC Plug Repairs

Tahir Gökçen†
ELORET Corporation, NASA Ames Research Center, MS 230-2, Moffett Field, CA 94035

George A. Raiche,‡ David M. Driver,* John A. Balboni, and Ryan D. McDaniel****
NASA Ames Research Center, Moffett Field, CA 94035

Computational simulations are used as an integral part of arc-jet testing from the planning stages of the arc-jet experiments through post-test analysis for increasingly complex test configurations. This paper reports two applications of such analysis: an analysis for reinforced carbon-carbon plug repair tests conducted in a NASA Ames arc-jet facility, and a feasibility study of full-scale Shuttle wing leading edge plug repair tests in the facility, where four possible configurations are investigated. For the plug tests, arc-jet flows over wedge models, with and without plugs mounted, and plugs differing in step height and diameters, are simulated. For the feasibility study, arc-jet flows of four test configurations are simulated, and based on the predicted test environments of these configurations, one is recommended for future arc-jet tests of full-scale plug repair. The present analyses comprise computational simulations of the nonequilibrium flowfield in the facility nozzle and test box as well as the flowfield over the models. These examples further demonstrate the value of computational simulations in planning and analysis of arc-jet tests.

Nomenclature

c_i	=	mass fraction of species i
h	=	enthalpy
$h_\circ$	=	total enthalpy
h_{pc}	=	maximum plug step height at the center
h_{pn}	=	plug step height at the leading edge
l	=	panel length in the wedge model
M	=	Mach number
M_e	=	Mach number at the boundary layer edge
r_{cy}	=	radius of a cylinder model
r_n	=	nose radius of a test article
r_p	=	plug radius
r_{pc}	=	plug corner radius
r_c	=	wedge or model corner radius
p	=	pressure
p_s	=	surface pressure
$p_\circ$	=	total or stagnation pressure
q_s	=	surface heat flux
$\bar{q}$	=	normalized heat flux, or heat augmentation factor
s_i	=	arc length coordinate

† Senior Research Scientist, Senior Member AIAA
‡ Research Scientist, Lead for Arc-Jet Test Design Office, Member AIAA
* Research Scientist, Principal Investigator for Ames RTF Arc-Jet Experiments, Member AIAA
** Aerospace Engineer, Member AIAA

T	=	temperature or translational-rotational temperature
T_s	=	surface temperature
T_v	=	vibrational or vibrational-electronic temperature
w	=	width of the wedge model
α	=	cylinder or model deflection angle
δ	=	boundary layer thickness
ϵ	=	hemispherical emissivity
ρ_e	=	density at the boundary layer edge
τ_s	=	surface shear

I. Introduction

Arc-jet facilities provide the primary means to test the performance of various types of thermal protection systems (TPS) used on the outer surfaces of spacecraft in an aerothermodynamic heating environment. Thermal, chemical and morphological stability of the TPS surface in locations such as the nose cap and wing leading edge is particularly important. In a high enthalpy arc-jet facility, a test gas, usually air or a mixture of nitrogen, oxygen and argon, is passed through an electric arc discharge where energy is added to the flow. The test gas is then expanded through a converging-diverging nozzle into an evacuated test chamber to produce high-enthalpy hypersonic flow. NASA Ames Research Center has a number of arc-jet facilities within its Arc-Jet Complex that have long been used in development and testing of TPS for entry vehicles such as the Space Shuttle Orbiter and planetary probes. [1–4]

Development of efficient real gas computational fluid dynamics (CFD) codes and advances in computer technology in recent years have enabled CFD analysis to become an integral part of arc-jet testing. Arc-jet test configurations have also evolved from simple coupon or panel geometries of the past to increasingly more complex test geometries designed for aerothermodynamic simulation, and computational simulations are used from the planning stages of the arc-jet experiments through post-test analysis. One example of such use of CFD analysis for a complex arc-jet test configuration was reported in Refs. 5-7. These arc-jet tests were conducted at Ames and designed to simulate the entry flight environment experienced by a wing leading edge (WLE) location of an entry vehicle where local heating is especially severe due to bow shock and wing shock interaction. In Refs. 5-7, pre-test CFD simulations showed that a pylon-shaped test article could provide flow characteristics comparable to flight predictions for a winged vehicle. Pre-test simulations were also performed to determine the arc-jet conditions necessary to approximate target boundary layer and surface quantities (temperature, pressure and shear) on a swept winged vehicle during hypersonic Earth entry. Finally, post-test simulations were used for interpretation of the test data and for code validation. [7]

The primary objective of the present paper is to report two recent applications of such CFD analysis in arc-jet testing. The first application includes an analysis for reinforced carbon-carbon (RCC) plug repair tests conducted in an Ames arc-jet facility. The Space Shuttle Return-to-Flight (RTF) program has been developing and testing several on-orbit repair techniques for potential cracks and holes on the Shuttle wing leading edge. The RCC plug repair is one of the promising repair techniques under development, and the RTF program sponsored several sub-scale and full-scale RCC plug repair concepts for tests in the Ames arc-jets. [8] Computational simulations are performed in order to support these arc-jet tests and to determine similarities/differences between the flight and test environments. Representative computational simulations used for analysis and interpretation of the arc-jet test data are presented. The second application is also in support of the RTF test program. A feasibility study of full-scale RCC plug repair tests for the Shuttle WLE is performed, and four test configurations in the Ames arc-jet facilities are studied using CFD simulations. As a result of the feasibility study, a particular full-scale test configuration for the RCC plug repair is recommended.

II. Arc-jet Facility

NASA Ames Research Center has several arc-jet facilities within its Arc-Jet Complex. The 60-MW Interaction Heating Facility (IHF) has the highest power rating within this Complex. It was originally constructed for testing of relatively large-scale models at the peak heating conditions of the Space Shuttle

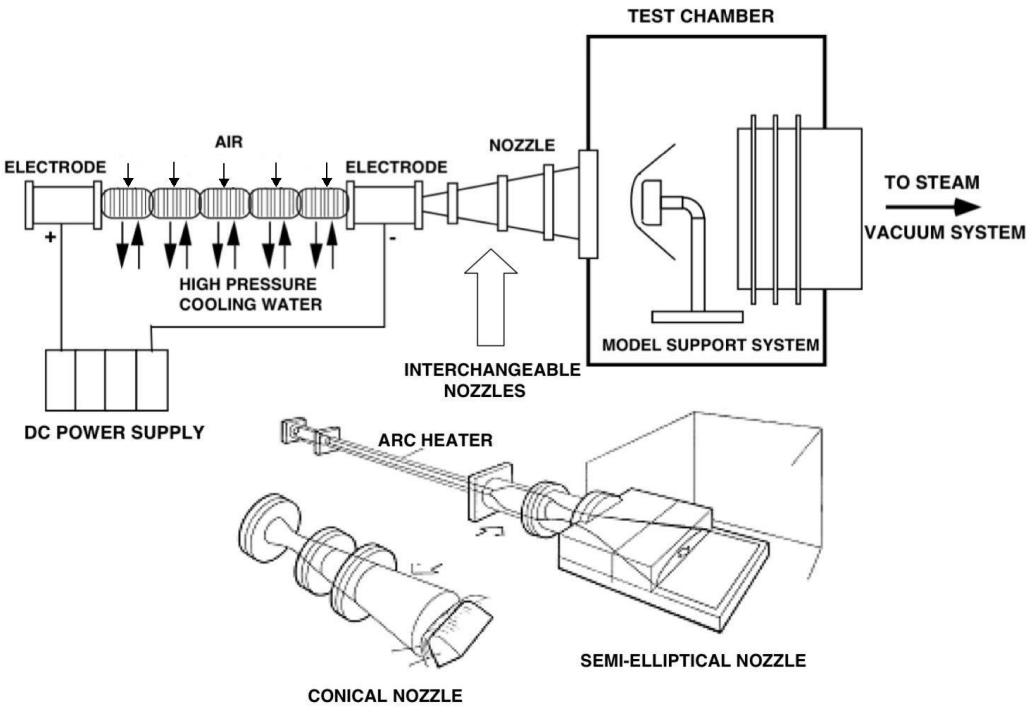

Figure 1. Sketches of NASA Ames 60-MW Interaction Heating Facility and its interchangeable nozzle configurations.

Orbiter vehicle entry. The IHF was used for the RCC plug repair tests, and it is also chosen for the feasibility study of a full-scale Shuttle WLE testing because of its capability to test relatively large size articles. Figure 1 shows a schematic diagram of the IHF and its nozzle configurations. The IHF consists of a constricted arc heater, a 60-MW DC power supply, interchangeable conical and semi-elliptical nozzles, a test chamber, and supplementary systems including steam ejector vacuum system, cooling-water system and data acquisition system. The IHF is designed to operate with a set of conical nozzles or a semi-elliptical nozzle at total pressures of 1-9 atm and total enthalpies of 7-47 MJ/kg (air).[1−4] The 60-MW constricted arc heater produces high-temperature test gas for both nozzles.

The conical nozzle configurations of the IHF are suitable for tests of stagnation coupon and blunted wedge test articles in hypersonic flow, while the semi-elliptical nozzle configuration is designed mainly for testing flat panels in hypersonic boundary-layer heating environments. Further information on the Ames IHF and other arc-jet facilities can be found in Refs. 1-4.

III. Computational Approach

The building blocks of the present computational analysis are (1) simulation of the nonequilibrium expanding flow in the IHF nozzles and supersonic jet, and (2) simulation of the nonequilibrium flowfield around arc-jet test articles.

The DPLR code[9,10] is used for computations of the nonequilibrium flow in the nozzle and flowfield around test articles. DPLR has been used extensively at Ames and elsewhere for hypersonic flight and planetary simulations, and its results have been favorably compared against a number of flight and ground-based experiments (e.g., see Refs. 11-15 and 7 and references therein).

The DPLR code provides various options for thermophysical models and formulation. For CFD simulations presented in this paper, the 3-D (or 2-D axisymmetric) Navier-Stokes equations, supplemented

Table 1. Chemical reaction set and forward rate parameters.

	$k_f = A\,\mathrm{T}^n\,e^{-\mathrm{T}_a/\mathrm{T}}$	A (cc/mol/s)	n	T_a (K)	Source
	Dissociation Reactions				
1.	$N_2 + M \rightleftharpoons N + N + M$	$7.0\text{x}10^{21}$	-1.6	113200	P(90) [17], P&L(95) [18]
	enhanced for M = N, O	$3.0\text{x}10^{22}$	-1.6	113200	P(90) [17], P&L(95) [18]
2.	$O_2 + M \rightleftharpoons O + O + M$	$2.0\text{x}10^{21}$	-1.5	59500	P(90) [17], P&L(95) [18]
	enhanced for M = N, O	$1.0\text{x}10^{22}$	-1.5	59500	P(90) [17], P&L(95) [18]
3.	$NO + M \rightleftharpoons N + O + M$	$5.0\text{x}10^{15}$	0.0	75500	P(90) [17], P&L(95) [18]
	enhanced for M = NO, N, O	$1.1\text{x}10^{17}$	0.0	75500	P(90) [17], P&L(95) [18]
	Exchange Reactions				
4.	$NO + O \rightleftharpoons O_2 + N$	$2.4\text{x}10^{13}$	1.0	19220	P&L(95) [18], H&S(84) [24]
5.	$N_2 + O \rightleftharpoons NO + N$	$1.8\text{x}10^{14}$	0.0	38400	P&L(95) [18], H&S(84) [24]

with the equations accounting for nonequilibrium kinetic processes, are used in the formulation. The governing equations are discretized using a finite volume approach. The convective fluxes are approximated using a modified Steger-Warming flux vector splitting. [16] The viscous fluxes are approximated by central differencing. The resulting difference equations of coupled fluid dynamics and chemistry are solved using an implicit Data-Parallel Line Relaxation (DPLR) method. More information on DPLR can be found in Wright et al. [9]

Thermochemical Model

A thermochemical model is an important part of nonequilibrium simulation of arc-jet flows as well as hypersonic flight. [17] However, validation of thermochemical models against arc-jet experiments has been limited in the literature: Park and Lee [18] have validated a multi-temperature model against a number of arc-jet experiments. Simplified sub-sets of this multi-temperature model, a two-temperature 12-species air model and a two-temperature 6-species air model (neutral chemistry), have been employed in simulations of flows in the Ames arc-jet facilities. [18–23,7]

The present calculations employ a 6-species air model (N_2, O_2, NO, N, O, Ar) for arc-jet flow, and the thermal state of the gas is described by two temperatures: translational-rotational and vibrational-electronic, within the framework of Park's two-temperature model. [17] The chemical reactions and forward reaction rates used in the model are given in Table 1. The forward reaction rates used are based on the works of Park [17] and Park and Lee. [18] Reverse reaction rates for all reactions are computed from the equilibrium constants using thermodynamic properties. For thermodynamic properties of species, NASA Lewis curve-fits are employed. [25] For surface recombination reactions of reaction-cured glass (RCG) coating, catalytic efficiency expressions developed by Stewart [26] are prescribed.

Modeling Assumptions and Boundary Conditions

In order to simulate the flowfield in an arc-jet facility, from the arc heater to the test section, several assumptions are made, and corresponding numerical boundary conditions are prescribed for CFD computations. These assumptions and boundary conditions are briefly described below.

(1) All simulations assume laminar flow.

(2) Nozzle simulations (both conical nozzle and semi-elliptical nozzle) are started from the nozzle throat. Total enthalpy and total pressure of the nozzle flow are important CFD inputs. Although total pressure (or arc-chamber pressure) is measured in the arc-jet tests, total enthalpy of the flow is deduced from the other measurements. Total enthalpy levels for conical nozzle test configurations are set such that CFD computations reproduce the calorimeter stagnation-point heat flux measurements. Similarly,

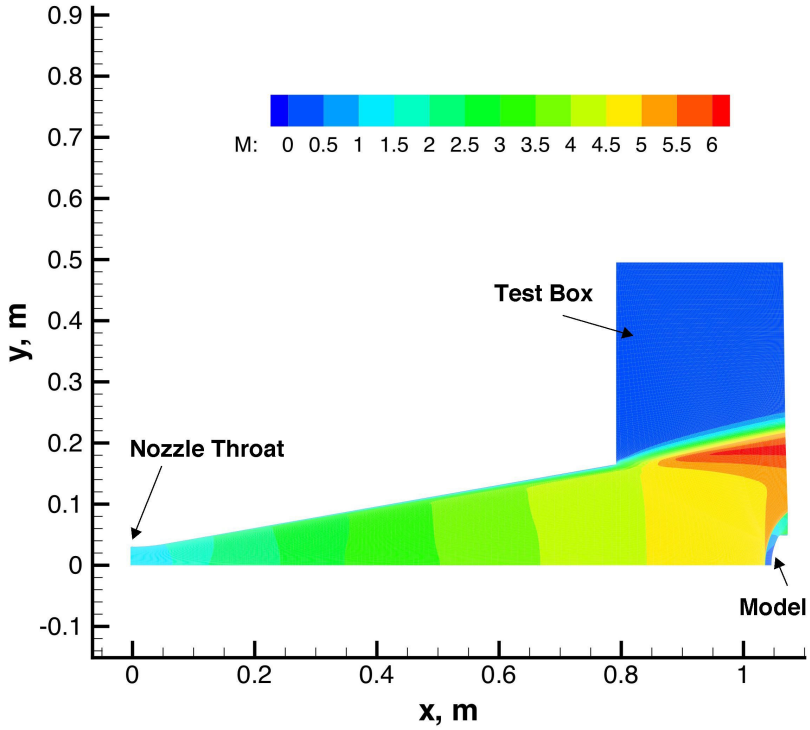

Figure 2. Computed Mach number contours: IHF 13-inch diameter nozzle flow downstream of the throat and flowfield over a calorimeter model (p_o = 674 kPa, h_o = 24.03 MJ/kg, and 8% Ar in air).

the enthalpy levels for semi-elliptical nozzle calculations are set to reproduce the calibration plate data, if available. In arc-jet testing, the extent of non-uniformity in the total enthalpy profile is deduced from the calorimeter and pitot pressure surveys taken at the nozzle exit and/or calibration plate measurements of pressure and heat flux in the semi-elliptical nozzle. Pitot and calorimeter surveys are usually performed for stagnation-point test configurations in which models are placed in a free jet downstream of the nozzle exit. For panel testing in a semi-free jet configuration, the calibration plates attached to the nozzle exit are used to assess flow uniformity. Total mass-averaged enthalpy is also estimated based on the arc-jet facility energy balance, which tends to be somewhat lower than the centerline total enthalpy (for arc-jet conditions of the IHF RCC wedge/plug tests, 15-20% typical). For simulations, a uniform total enthalpy profile at the throat is prescribed, and the centerline estimate of the total enthalpy is used. The flow properties at the throat are assumed to be those at thermochemical equilibrium. For 3-D flowfield simulations of arc-jet models in conical nozzles (e.g., 3-D wedge model and wedge model with a plug), the nozzle and model flowfields are decoupled, and predicted centerline conditions of the axisymmetric nozzle flow are used as freestream conditions for model flowfield simulations. For simulations of axisymmetric models in conical nozzles and semi-elliptical nozzle with a pylon, the nozzle and model flowfields are coupled and solved together.

(3) Water-cooled nozzle walls and copper wedge model surface are assumed to be fully catalytic to atomic recombination reactions at a constant temperature of 500 K.

(4) For all model surfaces that are not water-cooled, the catalytic efficiencies for surface recombination reactions are assumed to be those of RCG coating, and surface temperatures are calculated using the radiative equilibrium boundary condition ($\epsilon = 0.89$). The rationale for this is that surface catalysis of RCG coating is well understood,[26] and it is used as a reference material here in defining the arc-jet test heating environment. Also, it should be mentioned that RCG-based temperatures have been used in defining flight aerothermal heating environments of entry vehicles (e.g., for the Shuttle Orbiter TPS

Figure 3. Photographs of a wedge test in the IHF 13-inch conical nozzle flow and two wedge models tested.

in the RTF program). As a typical axisymmetric simulation, Figure 2 shows computed Mach number flowfield contours of the IHF 13-inch diameter conical nozzle flow with a calorimeter model placed downstream of the nozzle exit. Note that metric units are used throughout the paper, except that the IHF nozzles, wedges and plugs are referred to by their familiar names and identified with their dimensions in inches.

IV. Presentation of Computed Results

Computed results are presented in two sections: simulations in support of the IHF RCC plug repair tests and results of the feasibility study for full-scale Shuttle WLE testing.

Simulations of RCC plug repair tests

The Return-to-Flight program has been developing and testing several repair techniques for potential cracks and holes on the Shuttle wing leading edge. The RCC plug repair is one of the repair techniques that were evaluated, and the program has tested several RCC plug repair concepts in the Ames IHF. [8]

In the plug tests, two sets of plugs with 2.6-inch and 7-inch diameters were tested in the IHF 13-inch conical nozzle configuration. The plugs were mounted on flat surfaces of a wedge model holder inclined 30° to the flow in the jet. Two different wedge configurations (7-inch and 9-inch width wedges) were used, and several plug configurations were tested, with differences in the plug geometry and locations of the plugs on the wedge surface, etc. Figure 3 shows photographs of a wedge test in the IHF 13-inch conical nozzle and wedge models tested. This paper presents only computational simulations performed in support of these tests, and it will not include presentation of any experimental data. The reader is referred to Ref. 8 for further information on the IHF RCC plug repair tests.

The plug geometries tested varied during the IHF plug repair tests. For computational simulations, the plug geometry is idealized as a circular disk with varying step height profile (frisbee-like geometry), as shown in Fig. 4. A typical profile for the 2.6-in diameter plugs consists of a forward-facing step with a small corner radius ($r_{pc} = 0.254$ mm) followed by a circular arc to the center. For the 7-inch diameter

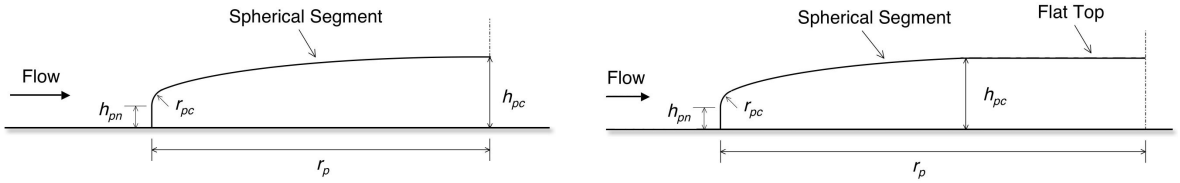

a) 2.6-inch diameter plugs b) 7-inch diameter plugs

Figure 4. Sketches of idealized plug geometries used in computations.

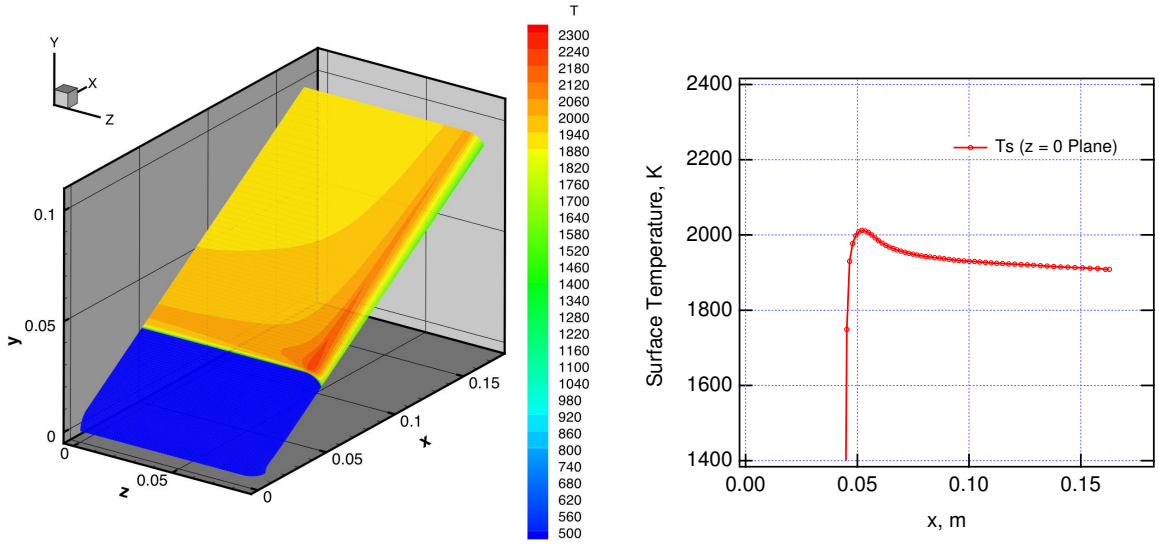

a) The 30° wedge model ($r_n = 0.95$ cm, $w = 17.78$ cm, $l = 18.42$ cm, $r_c = 0.635$ cm)

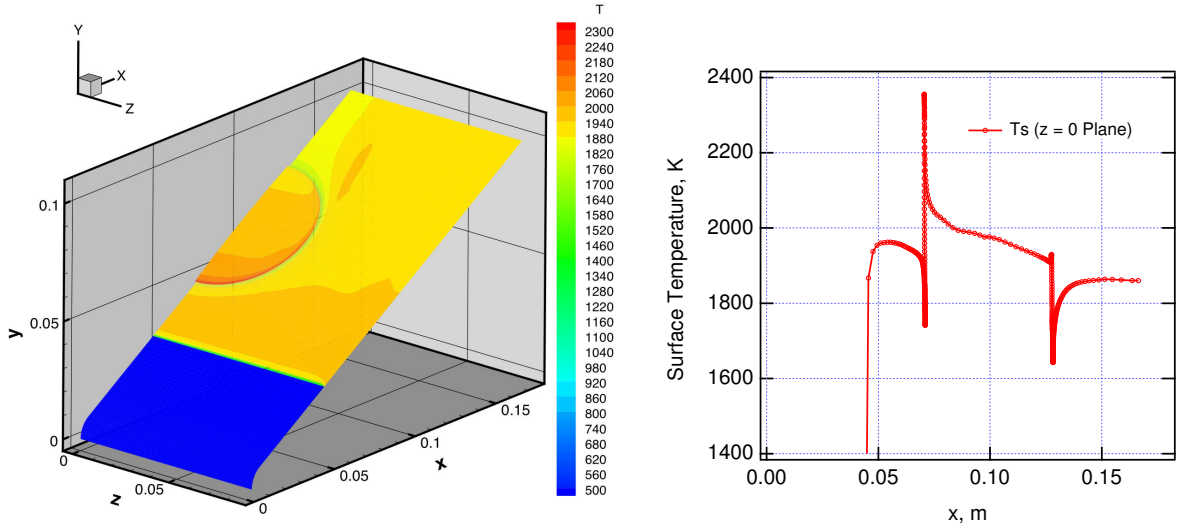

b) The wedge with the 2.6-inch diameter plug ($r_p = 3.302$ cm, $h_{pn} = 0.762$ mm, $h_{pc} = 1.905$ cm)

Figure 5. Computed surface temperature contours and centerline profiles of the 30° wedge model with and without the 2.6-inch diameter plug. In the contour plots, dimensions are in meters and the unit of temperature is K. Freestream conditions: IHF 13-inch nozzle flow with reservoir conditions of $p_o = 674$ kPa, $h_o = 24.03$ MJ/kg, and 8% Ar in air.

plugs, the plug profile is similar to the 2.6-inch plugs but the plug center also includes a flat top.

Initially, a 7-inch, 30° wedge ($r_n = 0.95$ cm, $w = 17.78$ cm, $l = 18.42$ cm, $r_c = 0.635$ cm) was used to test 2.6-inch diameter plugs. Figure 5 shows the computed surface temperature contours and centerline profiles of the calibration wedge and wedge with a 2.6-inch diameter RCC repair plug tested in the IHF. The wedge nose region is made of copper and it is water-cooled, hence it is simulated at a constant temperature of 500 K as shown. The computations predict significantly higher temperature at the leading edge of the plug in comparison to the corresponding portion of the smooth wedge. It should be mentioned here that since these simulations employ the radiative equilibrium boundary condition on

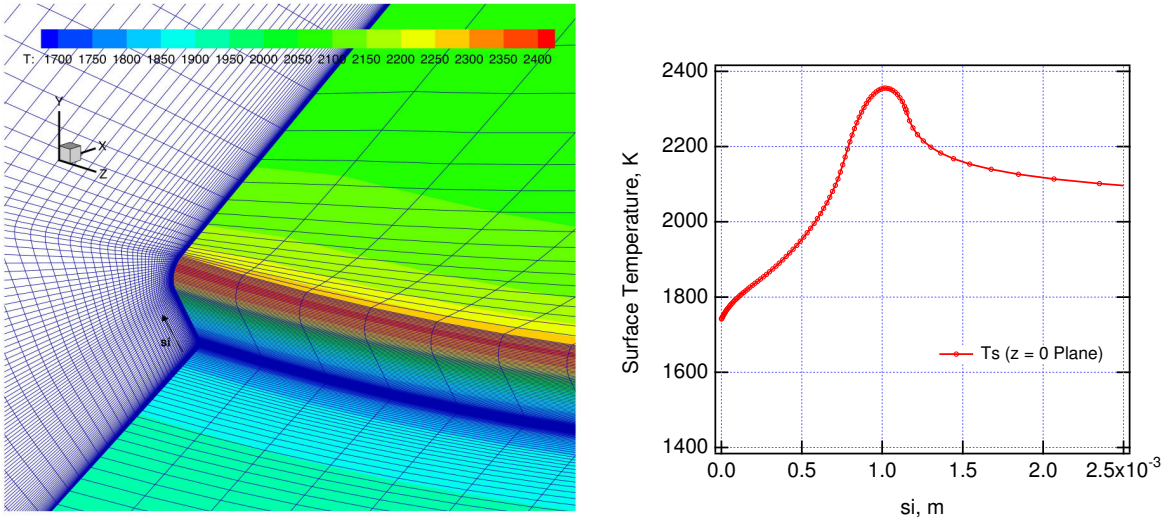

Figure 6. Computed surface temperature contours with the grid overlayed and centerline profile near the leading edge of the 2.6-inch diameter plug. Freestream conditions: IHF 13-inch nozzle flow with reservoir conditions of $p_o = 674$ kPa, $h_o = 24.03$ MJ/kg, and 8% Ar in air.

the surface of the plug and neglect the heat conduction effects, the peak heating rate at the plug leading edge is expected to be somewhat overpredicted. Effects of heat conduction on the plug surface temperature distribution have not been analyzed and are not quantified at this point. Nevertheless, the significant heating enhancement at the plug lip is observed by an infrared camera in the experiments.[8] Note that since the primary objective of plug simulations is to predict the heating enhancement due to the presence of the plug protuberance, the wedge edge effects are not included in the wedge/plug simulations (in contrast to the smooth wedge simulation). The temperature distributions near the plug lip, i.e., the temperature contours and centerline profile near the leading edge of the plug, are shown in Fig. 6. Part of the computational grid used to resolve the plug leading edge flow is also overlayed on the contour plots shown in Fig. 6. The surface pressure distributions over the 7-inch wedge models with and without the plug are shown in Fig. 7. Perturbations in computed pressure contours due to the presence of the plug are smaller than those for the temperature. Also, note that the decreasing centerline pressure along the wedge in Fig. 7a is an indication of the three dimensional edge effects. In Fig. 7b, the high pressure region in front of the plug due to stagnated, re-circulating flow and the low pressure region due to the flow expansion at the plug trailing edge are noticeable in the pressure contours.

A number of plug tests were also conducted using a 9-inch wide, 30° wedge holder ($r_n = 1.27$ cm, $w = 23.88$ cm, $l = 33.02$ cm, $r_c = 0.635$ cm). This wedge was primarily used to accommodate a 7-inch diameter plug. Arc-jet test conditions and the location of the plug on the wedge model were also different in comparison to the smaller wedge/plug tests. As representative simulation results, Figure 8 shows the computed surface temperature contours and centerline profiles for the 9-inch wedge and RCC repair plugs tested in the IHF. As in the smaller wedge, the wedge nose region is made of copper and it is water-cooled. As shown in the figure, two different size plugs were mounted on the wedge and tested: the 2.6-inch and 7-inch diameter plugs, both of which had approximately the same plug height at the plug lip (leading edge) and were located at about the same distance from the wedge plate leading edge. As shown in the line plots, the predicted temperatures at the 2.6-inch plug lip are higher than those of the 7-inch plug lip by about 4%.

Comparisons of normalized heat flux and pressure distributions for both plugs are shown In Fig. 9. The computed centerline heat fluxes are normalized by the smooth surface wedge values of the heat flux and pressure (80.4 W/cm^2 and 15.1 kPa), and the x coordinate is normalized by the plug diameter. The

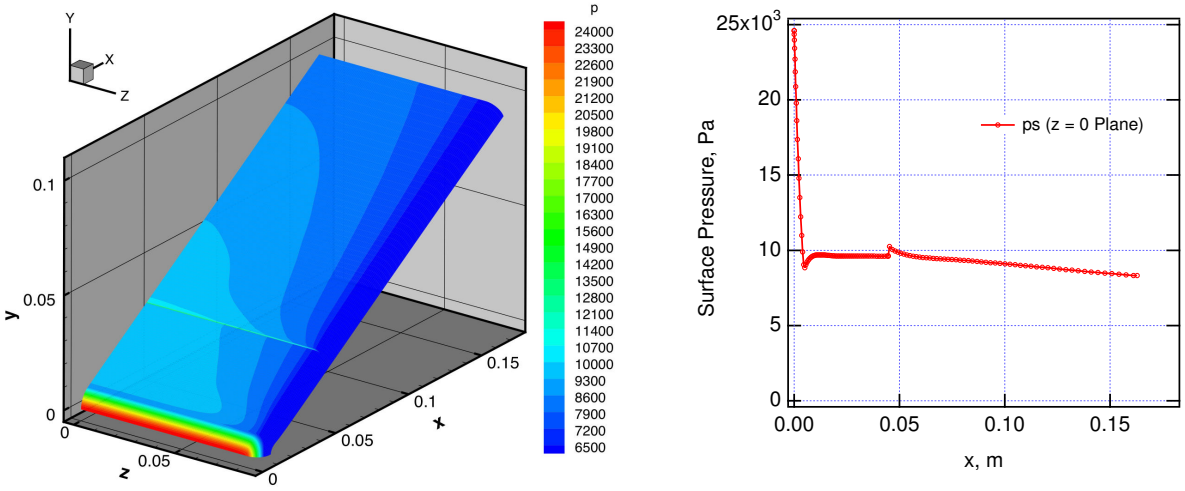

a) The 30° wedge model ($r_n = 0.95$ cm, $w = 17.78$ cm, $l = 18.42$ cm, $r_c = 0.635$ cm)

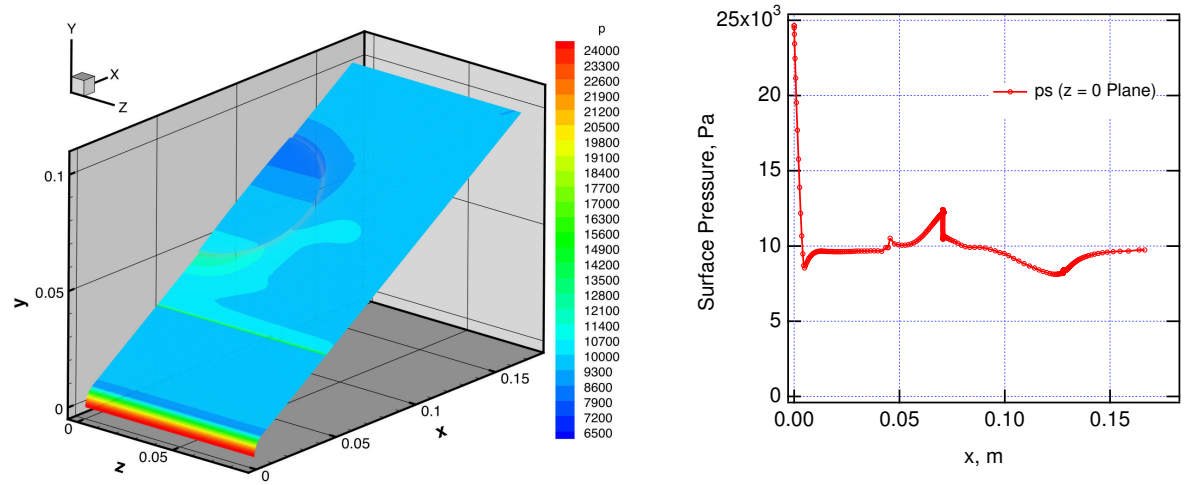

b) The wedge with the 2.6-inch diameter plug ($r_p = 3.302$ cm, $h_{pn} = 0.762$ mm, $h_{pc} = 1.905$ cm)

Figure 7. Computed surface pressure contours and centerline profiles of the 30° wedge model with and without the 2.6-inch diameter plug.

arc-length coordinate of the plug leading edge is not normalized. The normalized heat flux values, $\bar{q}$, represent augmentation in heat flux due to the presence of the plug, and therefore they are referred to as the heat augmentation factors (or "bump" factors). The computations predict that the heating rates on the plug leading edge are approximately twice the heating rate of the smooth wedge at the same location. Also, the leading edge peak heating rate for the 2.6-inch plug is about 15% higher than that for the 7-inch plug. This additional heating for the smaller plug may be attributed to higher cross flow gradients at the leading edge. The significant heating enhancements at the plug leading edges and the higher heating for the 2.6-inch plug than that for the 7-inch plug are all consistent with the experimental observations.[27] Also note that from Fig. 9a, the smaller plug not only has a higher heat flux at the lip but also experiences higher heat flux overall. As mentioned earlier, computations predict that the pressure field is much less influenced by the presence of the plug. Similar pressure rises at the leading edges of both plugs are predicted, and the differences in the predicted pressure distributions along the plug top

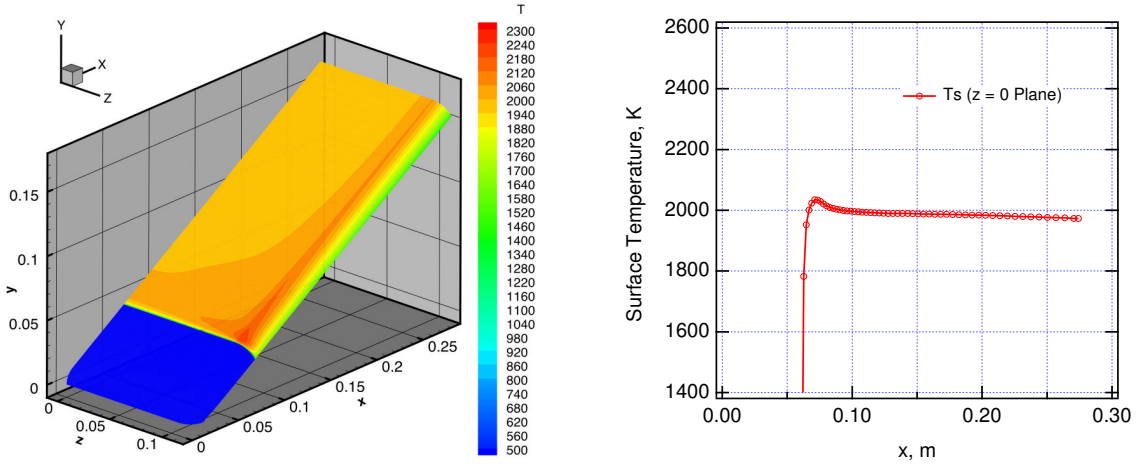

a) The 9-inch wide wedge ($r_n = 1.27$ cm, $w = 23.88$ cm, $l = 33.02$ cm, $r_c = 0.635$ cm)

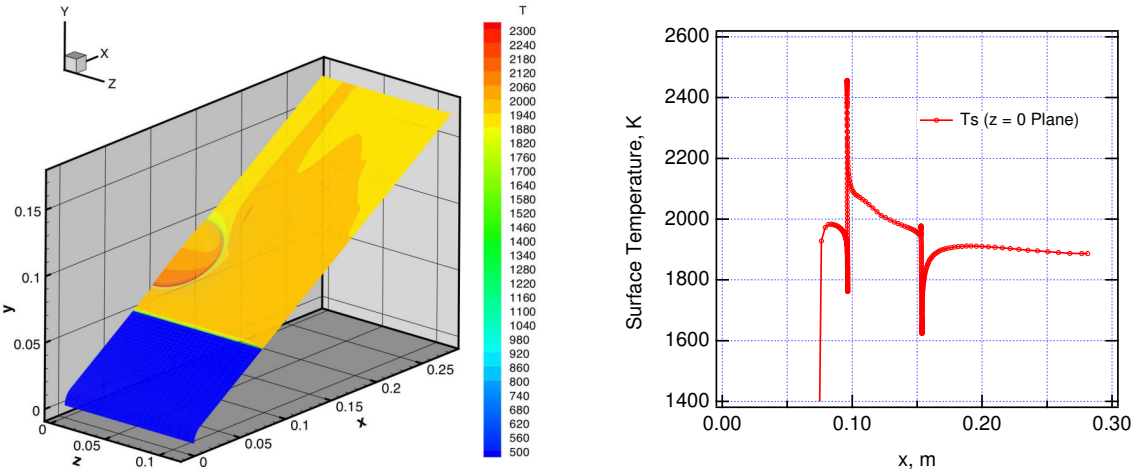

b) The 2.6-inch plug ($r_p = 3.302$ cm, $h_{pn} = 0.864$ mm, $h_{pc} = 2.007$ mm, $r_{pc} = 0.254$ mm)

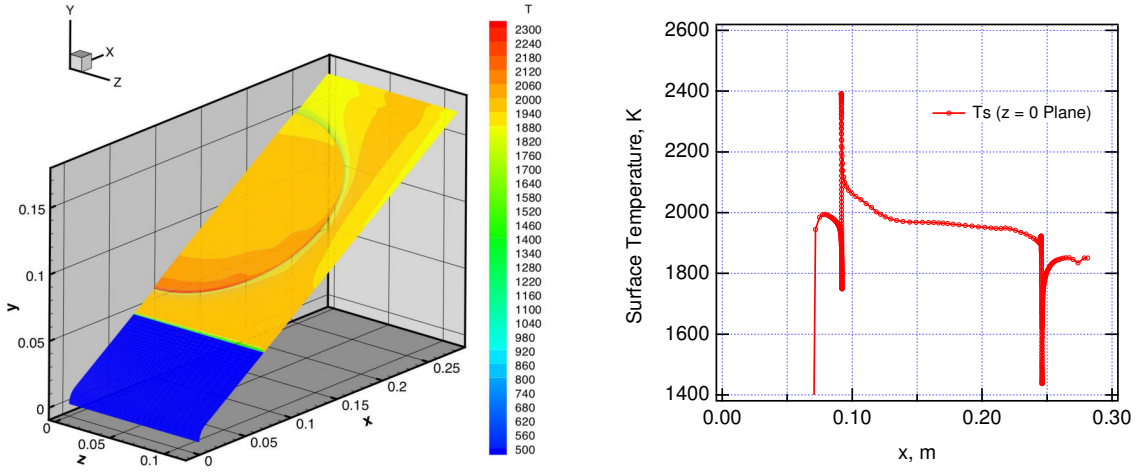

c) The 7-inch plug ($r_p = 8.890$ cm, $h_{pn} = 0.838$ mm, $h_{pc} = 1.981$ mm, $r_{pc} = 0.254$ mm)

Figure 8. Computed surface temperature contours and centerline profiles of the 30° wedge model with the two plugs. Freestream conditions: IHF 13-inch nozzle flow with reservoir conditions of $p_o = 842$ kPa, $h_o = 23.93$ MJ/kg, and 8% Ar in air.

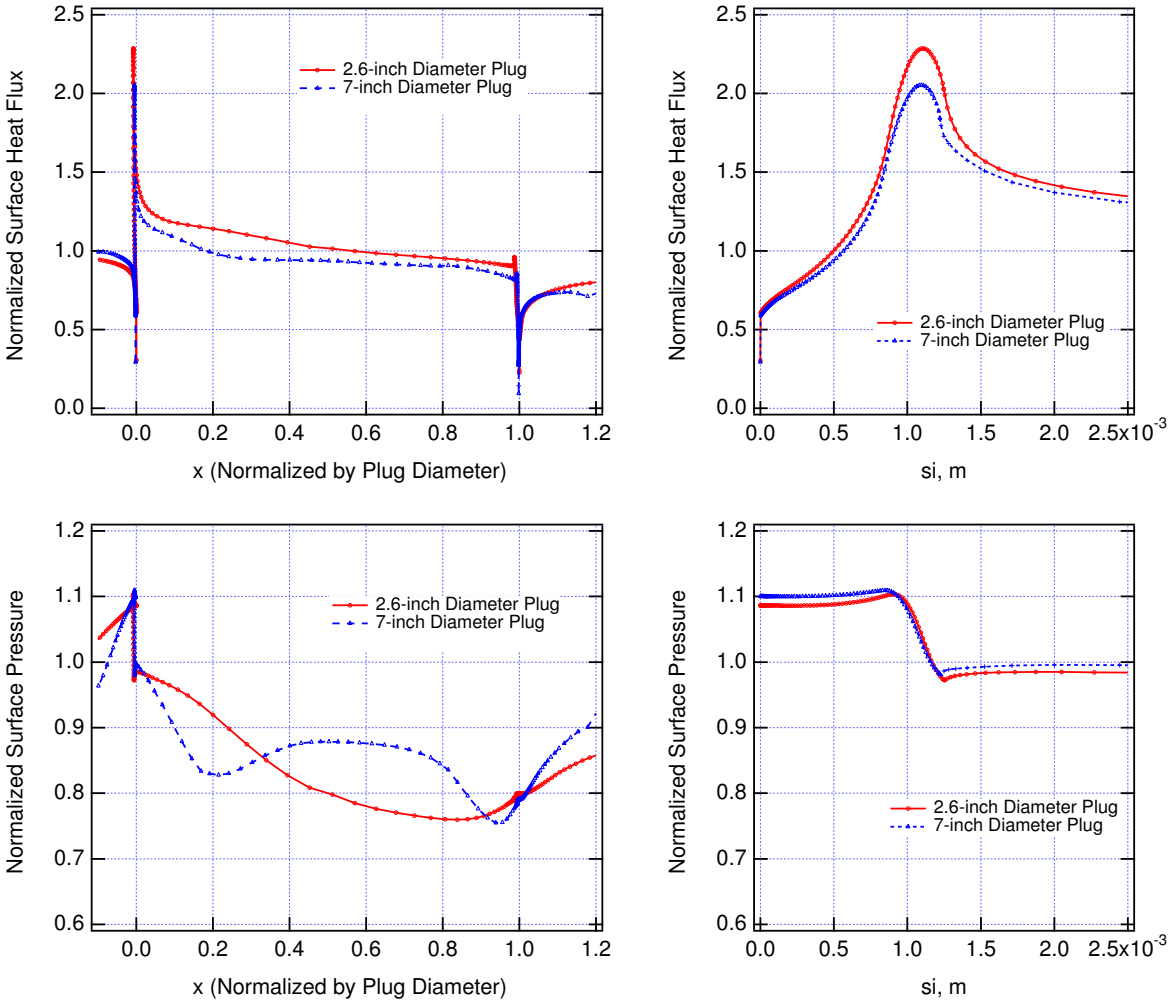

a) Along the plug centerline b) Near the plug leading edge

Figure 9. Normalized heat flux and pressure distribution along the centerline and near the leading edge of the 2.6-inch and 7-inch diameter plugs. Freestream conditions: IHF 13-inch nozzle flow with reservoir conditions of $p_o = 842$ kPa, $h_o = 23.93$ MJ/kg, and 8% Ar in air.

surfaces and near the trailing edges are likely caused by the differences in plug geometries (step height profiles and diameters).

The extent of the heating augmentation on the plug surface primarily depends on the plug geometry and aerothermodynamic environment factors. The important geometry parameters are the centerline plug profile, plug diameter, plug step height at the leading edge, and corner radius of the plug lip. The aerothermodynamic factors are boundary layer thickness, total enthalpy boundary layer profile upstream of the plug, thermochemical state of the high enthalpy flow, and the boundary layer edge properties such as M_e, h_{oe}, etc. However, it is outside the scope of this paper to perform computational studies of the heat augmentation factor with respect to all of these parameters. Nevertheless, it is expected that the plug step height is one of the most important geometry factors (or the the ratio of plug step height to the boundary layer thickness). Comparisons of normalized heat flux distributions for two 7-inch diameter plugs with different step heights are shown in Fig. 10. As may be expected, the heating augmentation at the plug leading edge is smaller for the plug that has a smaller step height. It is interesting to note that the heating augmentation factors for both plugs approach each other at the point about 20% downstream

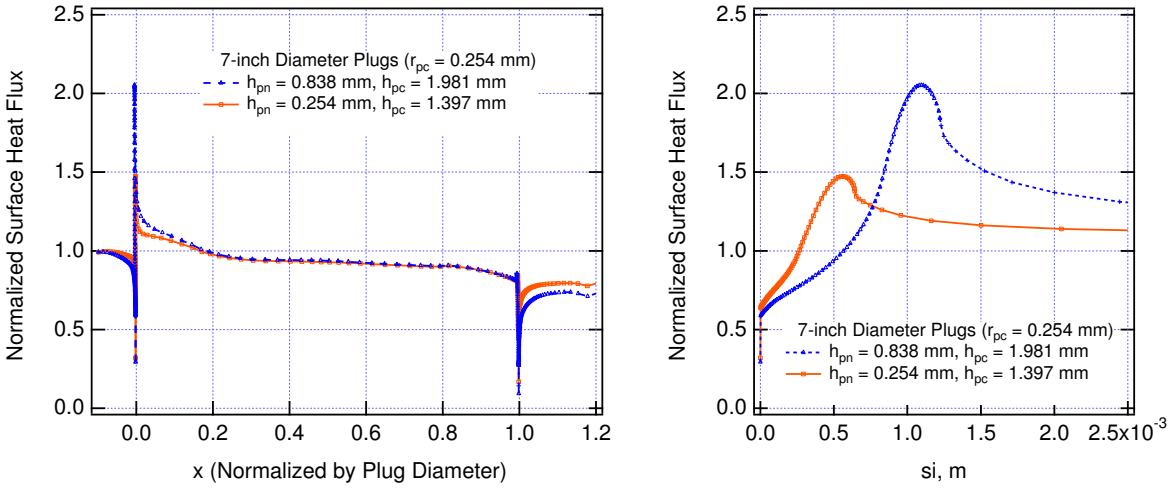

a) Along the plug centerline b) Near the plug leading edge

Figure 10. Normalized heat flux distribution along the centerline of two 7-inch diameter plugs. Freestream conditions: IHF 13-inch nozzle flow with reservoir conditions of p_o = 842 kPa, h_o = 23.93 MJ/kg, and 8% Ar in air.

of the plug lip (as shown in Fig. 10a). It appears that the effect of the step diminishes downstream, and the surface heat flux is mostly determined by the shape of the plug's top surface, which is the same for these two plugs.

For purposes of arc-jet test traceability to the flight environment, an important question often asked is whether or not a particular arc-jet test environment is more conservative (or severe) than that of flight. In order to answer this question, the heating augmentation factors in flight and arc-jet tests need to be investigated, perhaps by performing parametric studies with respect to plug geometry parameters and aerothermodynamic environment parameters for arc-jet and flight. Table 2 compares the computed arc-jet environment of the wedge flow shown in Fig. 8 with a representative flight environment of the Shuttle Orbiter in terms of surface quantities and boundary layer edge properties. Although such comparisons also need to be made for the other trajectory points, and the ratio of the plug step height to the boundary

Table 2. Comparisons of computed flight and arc-jet test environment parameters.

Environment Parameter	Flight/Shuttle WLE*	Arc-jet/Wedge**
δ, cm	1.41	0.56
h_p/δ	0.06 - 0.14	0.15 - 0.36
h_o, MJ/kg	23.5	24
M_e	3.08	1.47
ρ_e, kg/m^3	1.113×10^{-3}	6.297×10^{-3}
T_e, K	5418	6130
c_{Ne}	0.031	0.253
c_{Oe}	0.218	0.212
c_{Are}	0	0.08
p_s, kPa	2.1	15.9
τ_s, Pa	101	143
q_s, W/cm^2	41.3	80.4
$T_s(RCG)$, K	1692	1998

* Flight estimates are for the Shuttle WLE BP 5505 and obtained from D. Prabhu[28]

** Arc-jet estimates are for the wedge centerline location at x_s = 9.6 cm

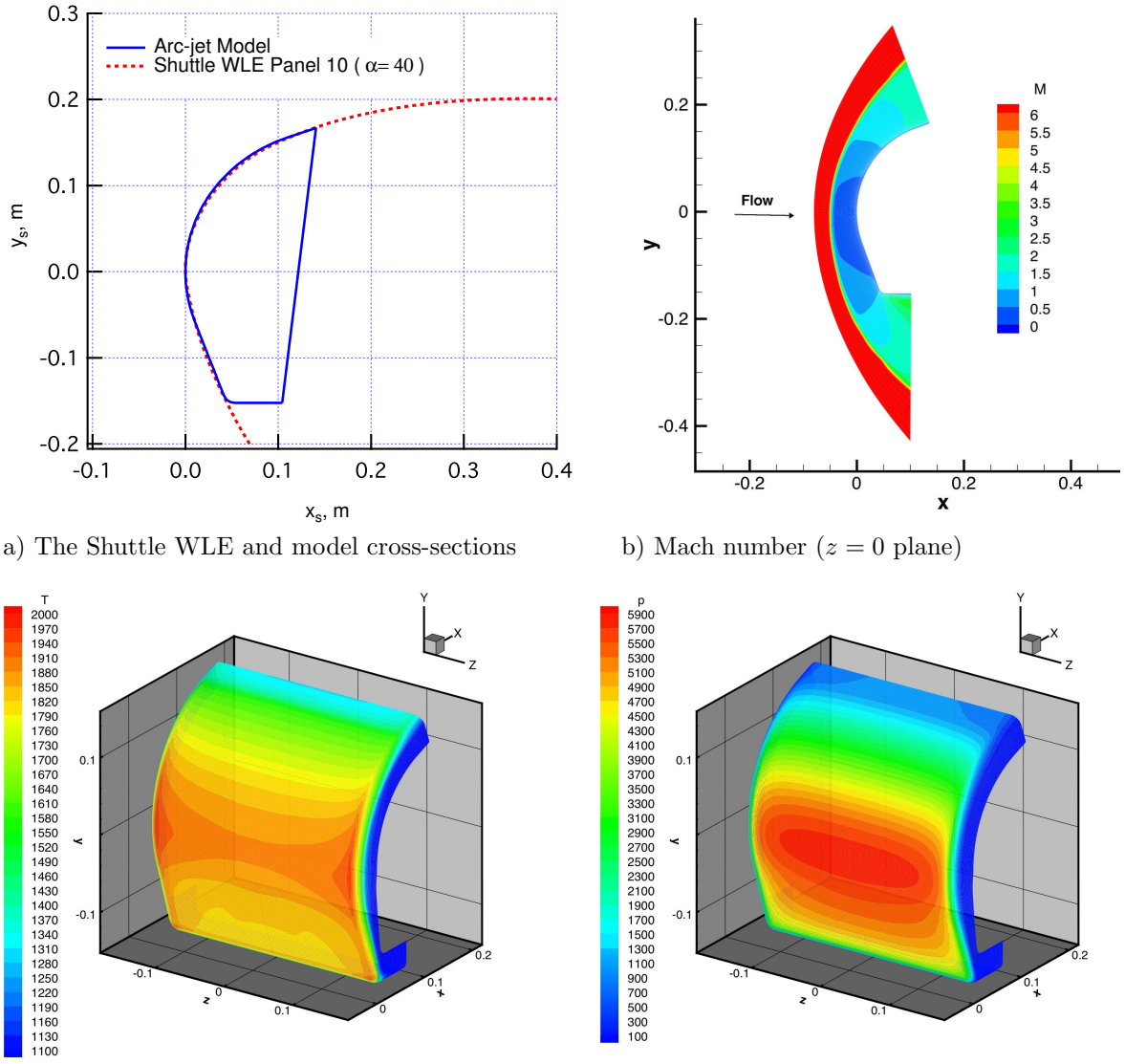

a) The Shuttle WLE and model cross-sections

b) Mach number ($z = 0$ plane)

c) Surface temperature, K

d) Surface pressure, Pa

Figure 11. Computed flowfield and surface contours of the Shuttle WLE stagnation test model (r_n = 17.15 cm, w = 30.48 cm, r_c = 1.27 cm). Freestream conditions: IHF 21-inch nozzle flow with reservoir conditions of p_o = 320 kPa, h_o = 29 MJ/kg, and 10% Ar in air.

layer thickness would clearly change along the heat pulse trajectory, at the trajectory point shown where the peak heating to the WLE occurs, it might be argued that the arc-jet test is more severe, purely based on comparisons of the computed heat fluxes and h_p/δ ratios.

Feasibility study for full-scale Shuttle WLE testing

It is well known that it is not possible to duplicate all of the similitude parameters of hypersonic flight in ground-based facilities. Therefore, one is forced to use a partial simulation approach in which a few selected simulation parameters are duplicated. The partial simulation parameters are usually combinations of dimensionless and dimensional parameters which are expected to be of primary importance to achieve arc-jet test objectives. Determination of these parameters requires characterizations of test and flight environments and some insight into the problem being studied.

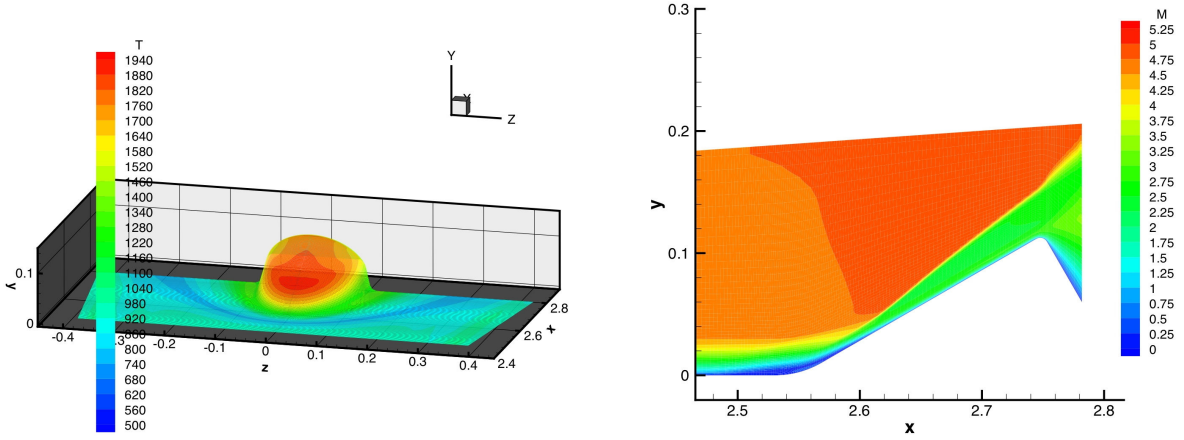

a) Temperature, K b) Mach number ($z = 0$ plane)

Figure 12. Computed surface temperature and Mach number contours of the semi-elliptical nozzle pylon model ($r_{cy} = 10.16$ cm, $l = 22.86$ cm, $r_{c1} = 7.62$ cm). Freestream conditions: IHF semi-elliptical nozzle flow with reservoir conditions of $p_o = 405$ kPa, $h_o = 18$ MJ/kg, and 10% Ar in air.

For full-scale Shuttle WLE RCC plug repair tests, a notional set of basic requirements may be stated: a full-scale arc-jet model must be able to hold a 7-inch diameter plug, and temperature and pressure on the smooth model surface (without plugs) must reach at least 1900 K and 5.75 kPa, respectively. In order to approximate the most severe Shuttle WLE flight environment in the arc-jet test as well as possible, the following secondary requirements are considered: (i) the model surface should be a curved surface similar to that of the Shuttle WLE; (ii) the flow at the boundary layer edge where the plugs are tested should be supersonic ($M_e = 2 - 3$); and (iii) the boundary layer thickness to plug height ratio should be similar to that of flight. It should be noted here that failure mechanisms of the RCC plugs on curved surfaces would likely be different from those on flat surfaces of the wedge due to thermal and mechanical stress differences. Also, interactions of the external flow and plug on curved surfaces would be different, and the heating augmentation would be higher on the curved surfaces due to increased velocity and pressure gradients. Thus modeling the curvature is highly desirable.

Feasibility of the following four options for the full-scale RCC plug repair arc-jet testing is investigated in this study: (1) conical nozzle Shuttle WLE stagnation test; (2) semi-elliptical nozzle pylon test; (3) conical nozzle wedge test; (4) conical nozzle swept-cylinder test. The IHF is chosen for the feasibility study of a full-scale Shuttle WLE testing because of the relatively large size of the intended test articles. The test article sizes given are limited by assuming a maximum model blockage ratio of 30% (ratio of the projected model area facing the flow to the area of the nozzle exit). For each option, sample results and key points about the test configuration are given below.

Option 1: Conical Nozzle Shuttle WLE Stagnation Test

This option involves testing actual Shuttle WLE panels with a 7-inch diameter plug. Figure 11 shows the computed flowfield and surface contours of the arc-jet WLE model. The model shape is made up of a truncated Shuttle WLE section profile at 40° angle of attack as shown in Fig. 11a, and it is not symmetric with respect to the x-z plane. Note that, for this and all the other models presented, the freestream flow direction coincides with the x-axis direction. The computed results show that the basic full-scale testing objectives could be met in the IHF 21-inch conical nozzle configuration. As stated, this is a stagnation point test similar to a flat-faced cylinder coupon test, but it provides a curved surface with temperature and pressure gradients. However, the boundary layer flow over the model is mostly subsonic and hence does not meet one of the secondary simulation requirements. A 7-inch diameter plug could only be placed near the stagnation point of the model, and interaction of the supersonic flowfield with the RCC plug lip would not be simulated.

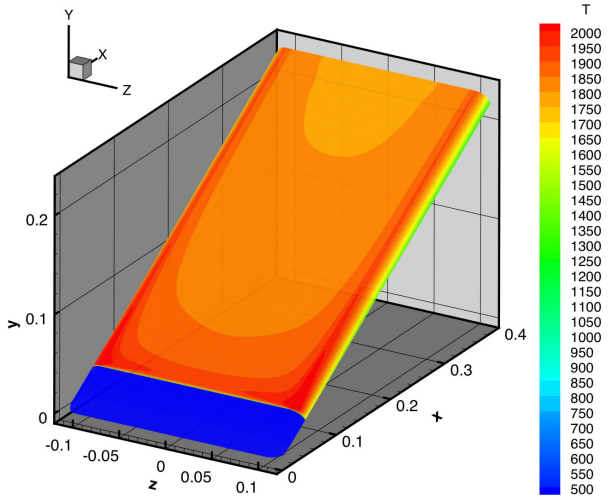

a) Surface temperature, K

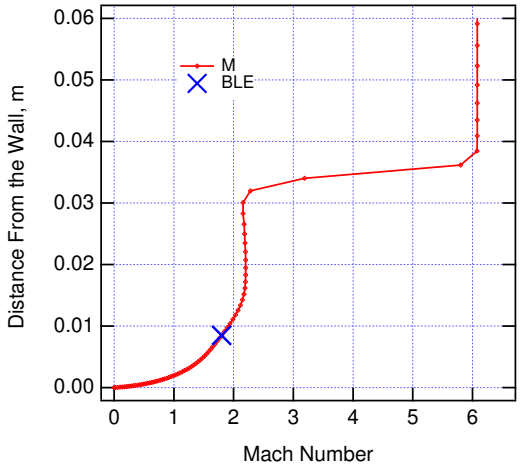

b) Mach number profile at $z_s = 0$, $x_s \approx 0.1$ m

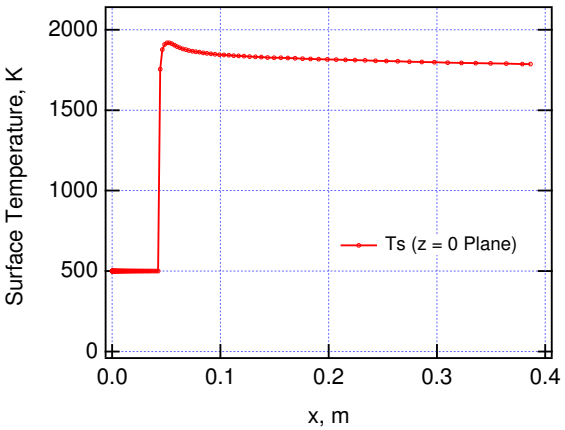

c) Surface temperature ($z = 0$ plane), K

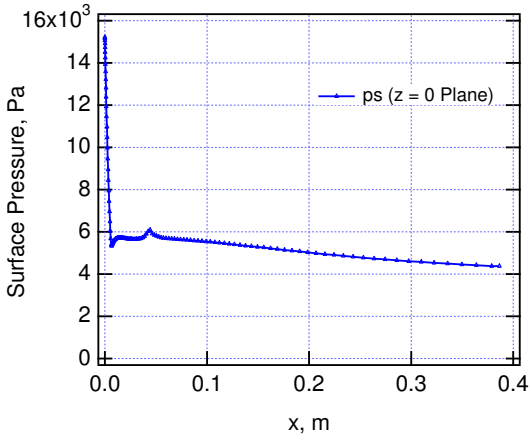

d) Surface pressure ($z = 0$ plane), Pa

Figure 13. Computed flowfield and surface quantities of the 30° wedge model (r_n = 1.27 cm, w = 22.86 cm, l = 45.72 cm). Freestream conditions: IHF 21-inch nozzle flow with reservoir conditions of p_o = 882 kPa, h_o = 26.2 MJ/kg, and 5% Ar in air.

Option 2: Semi-elliptical Nozzle Pylon Test

This option involves testing of swept-cylinder models in the IHF semi-elliptical nozzle flow (a swept pylon test). This test configuration is an excellent one for WLE testing, and is inspired by the swept pylon tests conducted by Stewart.[5–7] The computed results show that 10 to 15-cm radius pylons with 30° deflection angle would meet the stated test objectives in the IHF semi-elliptical nozzle configuration. Figure 12 shows computed surface temperatures and Mach number contours for a pylon model. This option not only meets the basic surface temperature and pressure requirements (surface pressure contours are not shown here), but also provides secondary test simulation parameters of interest: a curved surface, supersonic boundary layer edge Mach number (M_e = 2-3), surface shear stress, cross-flow characteristics, etc. However, the useful model length is significantly limited for pylons of 15 cm radius or larger, due to the limited extent of the flow in the y direction and to model blockage effects.

Option 3: Conical Nozzle Wedge Test

This option involves testing of blunted wedge models in the IHF 21-inch diameter conical nozzle.

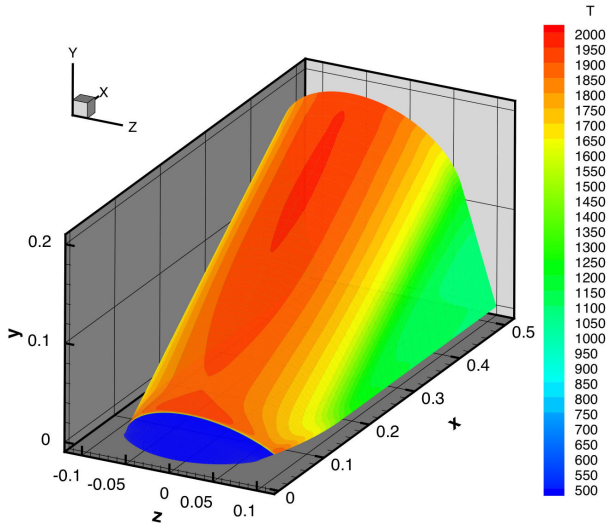

a) Surface temperature, K

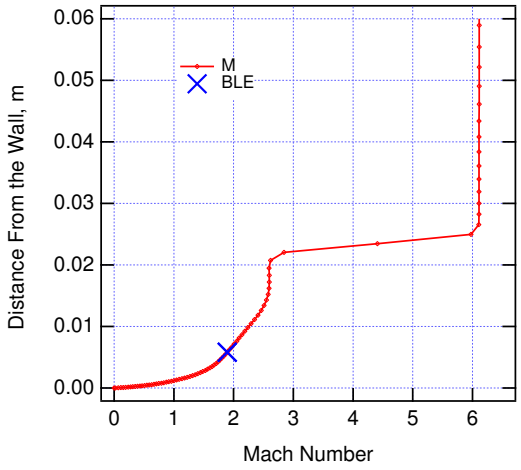

b) Mach number profile at $z_s = 0$, $x_s \approx 0.08$ m

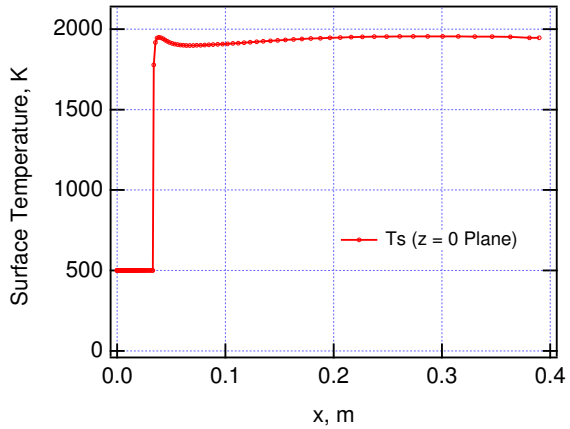

c) $z = 0$ plane surface temperature, K

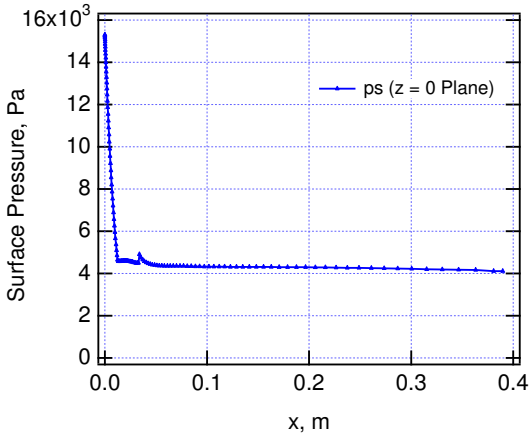

d) $z = 0$ plane surface pressure, Pa

Figure 14. Computed flowfield and surface quantitiies of the 30° swept-cylinder model ($r_n = 2.54$ cm, $r_{cy} = 10.16$ cm, $l = 45.72$ cm). Freestream conditions: IHF 21-inch nozzle flow with reservoir conditions of $p_o = 900$ kPa, $h_o = 23$ MJ/kg, and 10% Ar in air.

The test configuration has already been used in the RCC plug repair test earlier,[8] but for the full-scale tests, a larger wedge is used to accommodate a 7-inch diameter plug. The computed results show that basic test objectives could be met in the IHF 21-inch diameter conical nozzle. Figure 13 shows computed surface temperature contours for the wedge model and the centerline pressure and temperature profiles. Because of the relatively high heating rates, the nose region near the leading edge is water-cooled. Also shown in Fig. 13b is Mach number boundary layer profile at a representative test location, in which the boundary layer edge location (BLE) is determined as the location at which the total enthalpy of the flow is equal to 99.5% of the freestream total enthalpy when marching away from the wall. It should be noted here that the boundary layer edge Mach number is less than the Mach number value behind the oblique shock wave of the wedge model. This effect is due to the fact that the wedge model has a blunted nose, and it could be reduced by using wedge models with smaller nose radii. The RCC plug test program has used this wedge configuration in the IHF 13-inch diameter conical nozzle, mostly due to schedule and cost constraints.[8] Although this test provides a supersonic boundary layer edge condition, the Shuttle WLE curvature effects are not simulated.

Option 4: Conical Nozzle Swept-Cylinder Test

This option involves testing of blunted swept-cylinder models in the IHF 21-inch conical nozzle. The test configuration replaces the blunted wedge in Option 3 with a blunted swept-cylinder in order to simulate the WLE curvature effects. The computed results show that a 10 to 12-cm radius cylinder with 30° deflection angle would meet the basic test objectives in the IHF 21-inch nozzle configuration. Figure 14 shows computed flowfield and surface quantitities for the swept-cylinder model. The swept-cylinder model is blunted at the leading edge, and its nose region near the leading edge is water-cooled. This test configuration, similar to Option 2, enables investigation of the Shuttle WLE curvature effects with a supersonic Mach number at the boundary layer edge, and it also allows adjustment of the deflection angle as a practical flexibility to obtain certain surface conditions, if needed.

As mentioned earlier, in the feasibility study, the considered test articles imply model blockage area ratios of no more than 30% for the IHF 21-inch diameter nozzle configuration. Recently, successful blockage tests with a larger swept-cylinder model (17.78 cm radius) were conducted using the IHF 21-inch diameter nozzle,[29] indicating that a 50% blockage area ratio is feasible. The conclusions reached for the four test configurations still hold. In addition, since a blockage ratio of 50% appears to be tolerable, the IHF 13-inch diameter nozzle could be substituted and thus provide higher heat flux and pressure conditions for the plugs to be tested.

In summary of the feasibility study, Options 2 and 4 both provide good test configurations meeting the originally stated basic test requirements, and satisfying secondary test simulation parameters that wedge or stagnation configurations cannot meet. Note that the cylindrical cross-section in these configurations could be replaced by an asymmetric WLE shape similar to the one shown in the stagnation test configuration of Option 1. Determination of the test configuration from these two options would depend on various factors: boundary-layer thickness requirements upstream of the plugs, cross-flow and shear stress requirements, cost of the test, etc. These factors and requirements are of interest to the Shuttle RTF program office. At the present time, primarily due the model size limitations of Option 2, the swept-cylinder configuration of Option 4 is recommmended for future full-scale RCC plug repair tests.

V. Summary and Concluding Remarks

Two recent applications of CFD-based analysis in arc-jet testing are presented. The reported applications are simulations of the reinforced carbon-carbon plug repair tests conducted in a NASA Ames arc-jet facility, and a feasibility study of four possible configurations for full-scale Shuttle wing leading edge plug repair tests in the Ames facility.

Comutational simulations of arc-jet flows over wedge models, with and without plugs mounted, and plugs differing in step height and diameters, indicate that the heating rate augmentation due to the presence of a plug is significant. For the nominal 2.6-inch and 7-inch diameter plugs tested, computed heating rates on the plug leading edge are approximately twice the smooth wedge heating rate, and the leading edge heating rate for the 2.6-inch plug is about 15% higher than that for the 7-inch plug. The plug heating augmentation factor increases with increasing step height, but only near the plug leading edge. The simulations use a radiative equilibrium boundary condition on the plug surfaces and neglect heat conduction effects. Therefore, the peak heating rate at the plug leading edge is expected to be overpredicted relative to heat-conducting repair materials.

A feasibility study of full-scale Shuttle WLE testing at Ames arc-jets is also presented. A range of options appears feasible depending on the relative ranking of test requirements. From four possible arc-jet test configurations presented, a swept-cylinder configuration using an IHF conical nozzle is recommended as the best test configuration for simulating flight environment parameters.

CFD analysis provides estimates of environmental parameters that may be extremely difficult to measure in test (or flight). These properties, such as boundary layer thickness, edge Mach number, and shear are often critical parameters for TPS behavior. Computational simulations, when validated, can assist test planning, define arc-jet test environments for surface properties of TPS, reduce exploratory testing, and provide a framework for tracing the TPS performance from a ground test facility to flight.

Acknowledgments

The authors would like to thank the following people: Michael Wright for making the DPLR code available, Dinesh Prabhu for providing flight environment parameters, Dean Lester for discussions on arc-jet plug tests, and all of the Thermophysics Facilities Branch Members involved in the Arc-Jet Complex for providing information on the facilities and the IHF RCC plug repair tests, in particular, Frank Hui and Imelda Terrazas-Salinas. This work was funded by the NASA Space Shuttle Return-To-Flight Program. The support from NASA Ames Space Technology Division through contract NNA04BC25C to ELORET Corporation is gratefully acknowledged.

References

[1] Winovich, W., Balakrishnan, A., and Balboni, J., "Experimental and Analytical Derivation of Arc-Heater Scaling Laws for Simulating High-Enthalpy Environments for Aeroassisted Orbital Transfer Vehicle Application," *AIAA Paper 85-1006*, June 1985.

[2] Peterson, A. B., Nichols, F., Mifsud, B., and Love, W., "Arc Jet Testing in NASA Ames Research Center Thermophysics Facilities," *AIAA Paper 92-5041*, Dec. 1992.

[3] Terrazas-Salinas, I., and Cornelison, C., "Test Planning Guide for ASF Facilities," Thermophysics Facilities Branch, Space Technology Division, NASA Ames Research Center, March 1999.

[4] "Thermophysics Facilities Branch Fact Sheet," Thermophysics Facilities Branch, Space Technology Division, NASA Ames Research Center, Jan. 2005.

[5] Stewart, D. A., Squire, T., Gökçen, T., and Henline, W., "Arc-Jet Flight Simulation Tests for X-37 Wing Leading Edge TPS," X-37 Report for ARC 05 Task 02, Oct. 2004.

[6] Stewart, D. A., "Arc-Jet Flight Simulation Tests for X-37 Wing Leading Edge TPS," NASA TM (in preparation), 2006.

[7] Gökçen, T., and Stewart, D. A., "Computational Analysis of Semi-elliptical Nozzle Arc-jet Experiments: Calibration Plate and Wing Leading Edge," *AIAA Paper 2005-4887*, June 2005.

[8] Driver, D. M., Hui, F., Gökçen, T., Raiche, G. A., Balboni, J. A., Terrazas-Salinas, I., Mayeaux, B., Riccio, J., Lin, F., and Lester, D., "Aeroheating Testing Approach for Shuttle Wing Leading Edge Repair Concepts," *AIAA Paper 2006-3297*, June 2006

[9] Wright, M. J., Candler, G. V., and Bose, D., "Data-Parallel Line Relaxation Method for the Navier-Stokes Equations," *AIAA Journal*, Vol. 36, No. 9, pp. 1603-1609, Sept. 1998.

[10] Wright, M. J., "Data-Parallel Line Relaxation (DPLR) Code, Version 3.03," Private Commmunication, May 2003.

[11] Wright, M., Loomis, M., and Papadapoulos, P., "Aerothermal Analysis of the Project Fire II Afterbody Flow," *Journal of Thermophysics and Heat Transfer*, Vol. 17, No. 2, 2003, pp. 240-249; also AIAA Paper 2001-3065, June 2001.

[12] Wright, M. J., Prabhu, D. K., and Martinez, E. R., "Analysis of Afterbody Heating Rates on Apollo Command Modules, Part 1: AS-202," *AIAA Paper 2004-2456*, June 2004.

[13] Reuther, J. J., Prabhu, D. K., Brown, J. L., Wright, M. J., and Saunders, D. A., "Computational Fluid Dynamics for Winged Re-entry Vehicles at Hypersonic Conditions," *AIAA Paper 2004-2537*, June 2004.

[14] Olejniczak, J., Wright, M. J., Laurence, S, and Hornung H. J., "Computational Modeling of T5 Laminar and Turbulent Heating Data on Blunt Cones, Part 1: Titan Applications" *AIAA Paper 2005-0176*, Jan. 2005.

[15] Wright, M. J., Olejniczak, J., Brown, J. L., Hornung H. J., and Edquist, K. T., "Computational Modeling of T5 Laminar and Turbulent Heating Data on Blunt Cones, Part 2: Mars Applications," *AIAA Paper 2005-0177*, Jan. 2005.

[16] MacCormack, R. W. and Candler, G. V., "The Solution of the Navier-Stokes Equations Using Gauss-Seidel Line Relaxation," *Computers and Fluids*, Vol. 17, No. 1, 1989, pp. 135-150.

[17] Park, C., *Nonequilibrium Hypersonic Aerothermodynamics*, John Wiley & Sons, Inc., New York, 1990, Chap. 8.

[18] Park, C. and Lee, S. H., "Validation of Multitemperature Nozzle Flow Code," *Journal of Thermophysics and Heat Transfer*, Vol. 9, No. 1, 1995, pp. 9-16; also AIAA Paper 93-2862, July 1993.

[19] Gökçen, T., "Computation of Nonequilibrium Viscous Flows in Arc-Jet Wind Tunnel Nozzles," *AIAA Paper 94-0254*, Jan. 1994.

[20] Gökçen, T., Park, C. S., Newfield, M. E., and Fletcher, D. G., "Computational Simulation of Emission Spectra from Shock Layer Flows in an Arc-Jet Facility," *Journal of Thermophysics and Heat Transfer*, Vol. 12, No. 2, 1998, pp. 180-189; also AIAA Paper 97-0135, Jan. 1997.

[21] Gökçen, T., Park, C. S., and Newfield, M. E., "Computational Analysis of Shock Layer Emission Measurements in an Arc-Jet Facility," *AIAA Paper 98-0891*, Jan. 1998.

[22] Loomis, M. P., Polsky, S., Venkatapathy, E., Prabhu, D, and Hui, F. C. L., "Arc-Jet Semi-Elliptic Nozzle Simulations and Validation in Support of X-33 TPS Testing," *AIAA Paper 98-0864*, Jan. 1998.

[23] Loomis, M. P., and Palmer, G., "Pre-Flight CFD Analysis of Arc Jet and Flight Environments for the SHARP-B2 Flight Experiment," *AIAA Paper 2001-0982*, Jan. 2001.

[24] Hanson, R. K., and Salimian, S., "Survey of Rate Constants in the N/H/O System," *Combustion Chemistry*, edited by W. C. Gardiner, Jr., Springer-Verlag, New York, 1984, Chap. 6.

[25] Gordon, S., and McBride, B.J., "Computer Program for Calculation of Complex Chemical Equilibrium Compositions, and Applications. Analysis Part I," NASA RP-1311,1994.

[26] Stewart, D. A., "Surface Catalysis and Characterization of Proposed Candidate TPS for Access-to-Space Vehicles," NASA TM 112206, July 1997.

[27] Lester, D., Scientist, ATK Thiokol, Brigham City, UT, Private Commmunication, Feb 2006.

[28] Prabhu, D., Senior Research Scientist, ELORET, NASA Ames Research Center, Moffett Field, CA, Private Commmunication, 2005.

[29] Balboni, J. A., "Leading Edge Experiments in an Arc Jet with a Large Swept Cylinder," National Space and Missile Materials Symposium, Orlando, FL, 26-30 June 2006.